Cellular/Molecular

Alternative Splicing as a Molecular Switch for Ca^{2+}/Calmodulin-Dependent Facilitation of P/Q-Type Ca^{2+} Channels

Dipayan Chaudhuri,[1] Siao-Yun Chang,[3] Carla D. DeMaria,[2,4] Rebecca S. Alvania,[1] Tuck Wah Soong,[3,5] and David T. Yue[1,2]

Departments of [1]Neuroscience and [2]Biomedical Engineering, Johns Hopkins University School of Medicine, Baltimore, Maryland 21205, [3]National Neuroscience Institute, Singapore 308433, [4]Office of Technology Licensing, Georgetown University, Washington, DC 20057, and [5]Department of Physiology, National University of Singapore, Singapore 117597

Alternative splicing of the P/Q-type channel ($Ca_V2.1$) promises customization of the computational repertoire of neurons. Here we report that concerted splicing of its main α_{1A} subunit, at both an EF-hand-like domain and the channel C terminus, controls the form of Ca^{2+}-dependent facilitation (CDF), an activity-dependent enhancement of channel opening that is triggered by calmodulin. In recombinant channels, such alternative splicing switches CDF among three modes: (1) completely "ON" and driven by local Ca^{2+} influx through individual channels, (2) completely "OFF," and (3) partially OFF but inducible by elevated global Ca^{2+} influx. Conversion from modes 1 to 3 represents an unprecedented dimension of control. The physiological function of these variants is likely important, because we find that the distribution of EF-hand splice variants is strikingly heterogeneous in the human brain, varying both across regions and during development.

Key words: **$Ca_V2.1$; EF hand; short-term synaptic plasticity; Ca^{2+}-dependent inactivation; developmental alternative splicing; exon 37**

Introduction

Alternative splicing can vastly diversify the function of single genes, potentially tailoring molecular phenotype to local environment (Modrek and Lee, 2002). In the brain, this diversity can impact the behavior of neural systems (Grabowski and Black, 2001). Within individual neurons, splicing is amply documented for molecules constituting major Ca^{2+} entry pathways, such as the Ca_V1–2 family of Ca^{2+} channels (Lipscombe et al., 2002; Lipscombe and Castiglioni, 2003). In particular, P/Q-type ($Ca_V2.1$) Ca^{2+} channels, the predominant triggers of CNS neurotransmitter release (Wheeler et al., 1994; Dunlap et al., 1995; Wheeler and Tsien, 1999), possess principal α_{1A} subunits that are spliced extensively (Mori et al., 1991; Starr et al., 1991; Ophoff et al., 1996; Zhuchenko et al., 1997; Bourinet et al., 1999; Soong et al., 2002; Tsunemi et al., 2002). Splicing at certain loci has been seen to impact P/Q-type channel pharmacology and gating (Bourinet et al., 1999), as well as expression (Soong et al., 2002). However, the functional consequences of variation have only been examined at a restricted subset of sites (Fletcher et al., 1996; Ligon et al., 1998; Bourinet et al., 1999; Hans et al., 1999; Krovetz et al., 2000; Toru et al., 2000; Soong et al., 2002). In numerous cases, the potential neurobiological impact of P/Q-type channel splice variation remains uncharted.

This study concerns the potential for splicing of P/Q-type channels to affect their regulation by calmodulin (CaM). CaM exerts two opposing effects, initially promoting Ca^{2+}-dependent facilitation (CDF) of channel opening and then inducing Ca^{2+}-dependent inactivation (CDI) of opening (Lee et al., 1999; DeMaria et al., 2001). CDF and CDI rapidly alter the amplitude of recombinant P/Q-type Ca^{2+} currents evoked by repetitive physiological stimuli (Lee et al., 2000; DeMaria et al., 2001). These regulatory processes may thus contribute to short-term synaptic plasticity (Borst and Sakmann, 1998; Cuttle et al., 1998; Forsythe et al., 1998; Borst and Sakmann, 1999) and thereby the computational potential of the brain (Abbott et al., 1997; Tsodyks and Markram, 1997; Tsodyks et al., 1998).

Of particular interest are α_{1A} splice variants within structural determinants of CaM–channel regulation. Specifically, splicing of exon 37 produces two variants of an EF-hand-like domain (see Fig. 1, EFa and EFb) (Zhuchenko et al., 1997; Bourinet et al., 1999; Krovetz et al., 2000; Soong et al., 2002), a region implicated by mutagenesis as critical for CaM regulation of related L-type ($Ca_V1.2$) channels (de Leon et al., 1995; Zuhlke and Reuter, 1998; Peterson et al., 2000; Kim et al., 2004). Unlike classic EF hands (Tufty and Kretsinger, 1975), the L-type EF hand (Babitch, 1990) might not bind Ca^{2+} but may instead transduce Ca^{2+}–CaM binding into channel modulation (Peterson et al., 2000; Kim et al., 2004). Because sequence alignments of the corresponding

Received May 4, 2004; revised May 26, 2004; accepted May 26, 2004.

This work was supported by a National Institutes of Health (NIH) Medical Scientist Training Program predoctoral fellowship (D.C.) and grants from NIH (D.T.Y.) as well as the National Medical Research Council (T.W.S.) and the Biomedical Research Council (T.W.S.).

Correspondence should be addressed to David T. Yue, Department of Biomedical Engineering, 1721 East Madison Street, Baltimore, MD 21205. E-mail: dyue@bme.jhu.edu.

DOI:10.1523/JNEUROSCI.1712-04.2004

 0270-6474/04/246334-09$15.00/0

segments of the L- and P/Q-type channels clearly suggest a common heritage (de Leon et al., 1995), could splicing of the analogous α_{1A} EF-hand-like region impact CaM regulation of P/Q-type channels? Here, we find that such EF-hand variation acts as a molecular switch for CDF while leaving CDI unaffected. Additionally, we show that the distribution of α_{1A} EF-hand splice variants is highly variable across the human brain in both space and time, suggesting widespread usage of this molecular switch.

Materials and Methods

Transient transfection. Methods were adapted from previous studies (DeMaria et al., 2001). To generate functional P/Q-type channels, we cotransfected plasmids encoding the human α_{1A} ($\alpha_1$2.1) pore-forming subunit and β_{2a} and $\alpha_2\delta$ accessory subunits, along with the simian virus 40 T antigen, into human embryonic kidney 293 (HEK293) cells by a calcium phosphate protocol (Dhallan et al., 1990). The β_{2a} subunit reduces voltage inactivation, allowing a closer examination of Ca^{2+}-dependent processes. The plasmid encoding the β_{2a} subunit also encoded a green fluorescent protein sequence that followed an internal ribosomal entry site. This construct thus allowed successfully transfected HEK293 cells to be identified by fluorescence. The T antigen permits plasmid replication in HEK293 cells, thereby enhancing expression of products encoded by transfected plasmids. The $\alpha_1$2.1 clone was a gift from Dr. Terry Snutch (University of British Columbia, Vancouver, Canada) (Sutton et al., 1999), and its splice variant content has been engineered to the following (Soong et al., 2002): Δ10A (+G); $16^+/17^+$; 17 (−VEA); -31^*(−NP); 37a (EFa) or 37b (EFb); $43^+/44^-$; Δ47 or 47+, where +G, −VEA, and −NP refer to splice variants with the inclusion (+) or omission (−) of amino acids specified by the single-letter code.

Electrophysiology. Two to 4 d after transfection of HEK293 cells, whole-cell current traces were recorded at room temperature. To examine CDI and CDF, we used a bath solution containing (in mM): 140 TEA-$MeSO_3$, 10 HEPES, and 5 $CaCl_2$ or $BaCl_2$, pH 7.4 (300–310 mOsm). We used the following internal solution (in mM): 135 Cs-$MeSO_3$, 5 $CsCl_2$, 0.5 EGTA, 1 $MgCl_2$, 4 MgATP, and 10 HEPES, pH 7.4 (290–300 mOsm). For certain experiments (see Fig. 6), we used a 10 mM concentration of the fast Ca^{2+} chelator BAPTA instead of 0.5 mM EGTA. All reagents were purchased from Sigma (St. Louis, MO).

Currents were recorded and filtered at 2 kHz bandwidth using an Axopatch 200A (Axon Instruments, Foster City, CA) amplifier and custom data-acquisition programs written by our laboratory. Data were analyzed off-line using custom programs written in Matlab (MathWorks, Natick, MA) and Excel (Microsoft, Seattle, WA). For statistical analysis, we used the *t* test, applying the Bonferroni correction when comparing across multiple groups (Glantz and Slinker, 1990).

Transcript scanning. According to previously described methods (Soong et al., 2002), we used PCR to amplify the exons flanking the EF hand from the following eight human cDNA libraries: whole brain (7187-1; Clontech, Palo Alto, CA), fetal brain (7129-1), amygdala (7190-1), cerebellum (7120-1), cerebral cortex (7110-1), hippocampus (7169-1), substantia nigra (7193-1), and thalamus (7188-1). The forward primer hEF5580U20 (5′-GGGAAACCGTGTGATAAGAA-3′) and the reverse primer hEF5975L15 (5′-GCTGTGCGGATCAGA-3′) were used for the amplification of a 410 bp fragment from the cDNA libraries. The reaction mix consisted of a 200 μM concentration of deoxy-ribose-NTPs (dNTPs), a 100 nM concentration of primers, 2.5 U of Taq DNA polymerase (Roche, Hertfordshire, UK), 1× PCR buffer with Mg^{2+} (Roche), and 0.5 μl of QUICK-clone human cDNA (Clontech) in a final volume of 25 μl. The cycling profile was set as follows: initial denaturation of template DNA at 94°C for 2 min, five touch-down cycles of denaturation at 94°C for 30 sec, annealing at 58–54°C for 40 sec, and extension at 72°C for 1 min, followed by 30 cycles of denaturation at 94°C for 30 sec, annealing at 53°C for 40 sec, and extension at 72°C for 1 min. The final extension was performed at 72°C for 10 min.

The amplicon represents the pool of both EFa and EFb cDNA forms. The fragment was gel purified, cloned into pDrive (Qiagen, Hilden, Germany), and transformed into *Escherichia coli* DH10B cells by electroporation. We identified clones by blue–white selection and then cultured them in 96 well microtiter plates. In general, a number of plates of white transformants were collected for each cDNA library.

Next, nested PCR was performed directly on the clones using an exon 36-specific forward primer, hEF5702U18 (5′-CGTCATCATGGACAACTT-3′), and either the exon 37a-specific primer EF1a.2-L20 (5′-ATATTACTCGTAATAAACTG-3′) or the exon 37b-specific primer EF1b.1-L20 (5′-GGGCGGAGACATGTGTCTCA-3′). The expected sizes of the EFa-specific and EFb-specific amplicons are 154 and 175 bp, respectively. The reaction mix consisted of a 50 μM concentration of dNTPs, a 50 nM concentration of each primer, 0.625 U of Taq polymerase (Promega, Madison, WI), 1× PCR buffer (Promega), 2 μM (for EFa screening) or 1 μM (for EFb screening) $MgCl_2$, and 1 μl of culture in a final volume of 25 μl. The cycling profile was set as follows: initial denaturation of template DNA at 94°C for 5 min, five touch-down cycles of denaturation at 94°C for 30 sec, annealing at 59–55°C for 40 sec, and extension at 72°C for 30 sec, followed by 30 cycles of denaturation at 94°C for 30 sec, annealing at 53°C for 40 sec, and extension at 72°C for 1 min. The final extension was performed at 72°C for 10 min

All PCR products were visualized in a 1.5% agarose gel. Only clones that were positive for EFa and negative for EFb, or vice versa, were taken to be confirmative results. All ambiguous results were disregarded. Accuracy of the exon-specific PCRs was verified by spot-checking clones by direct sequencing. Tabulation of the number of positives for each splice-specific PCR produced a ratio of EFa- versus EFb-containing transcripts in the various libraries.

Results

Splicing of the EF-hand domain as a molecular switch for CDF

For reference, we first considered a familiar variant of P/Q-type channels, composed of α_{1A} subunits containing both the EFa version of exon 37 and the longer carboxyl tail encoded by exon 47 [EFa/47+] (Fig. 1). Here, and for all recombinant channel expression experiments, α_{1A} was coexpressed with accessory β_{2a} and $\alpha_2\delta$ subunits in HEK293 cells. This genre of P/Q-type channels, closely similar to those investigated previously (DeMaria et al., 2001; Soong et al., 2002), would be expected to manifest robust CDF and CDI, characterized as follows. Indeed, with Ca^{2+} as the charge carrier, CDF was readily apparent as a slow phase of increasing Ca^{2+} current seen during short (50 msec) test depolarizations (Fig. 2*A*, arrow, gray trace). When channels were facilitated by Ca^{2+} entry during a preceding voltage prepulse, ensuing currents activated rapidly to the facilitated level during the test pulse (black trace). To quantify the facilitation produced by the prepulse, we integrated the difference (ΔQ) between normalized test-pulse currents in the absence and presence of a prepulse, and this integral was used to determine the relative facilitation (*RF*) induced by the voltage prepulse (see supplemental information, available at www.jneurosci.org/cgi/content/full/24/28/6334/DC1). Reassuringly, *RF* demonstrated a bell-shaped dependence on prepulse voltage (Fig. 2*B*, filled circles), as expected for a genuine Ca^{2+}-driven process (Brehm and Eckert, 1978). In contrast, as expected from the strong preference of CaM for Ca^{2+} over Ba^{2+} (Chao et al., 1984), there was little evidence of such prepulse facilitation with Ba^{2+} as the charge carrier, either in exemplar traces (Fig. 2*A*) or in population averages (Fig. 2*B*, open circles). The small, monotonic increase in *RF* seen with Ba^{2+} (Fig. 2*B*) reflected weak background G-protein modulation (DeMaria et al., 2001). Thus, to index pure CDF, we used the difference between Ba^{2+} and Ca^{2+} *RF* relationships (*g* value of ~0.23) after a 20 mV prepulse.

When viewed over longer (1 sec) depolarizations, the same P/Q-type channels [EFa/47+] gave strong evidence of an opposing CaM-mediated regulatory process, CDI. This manner of reg-

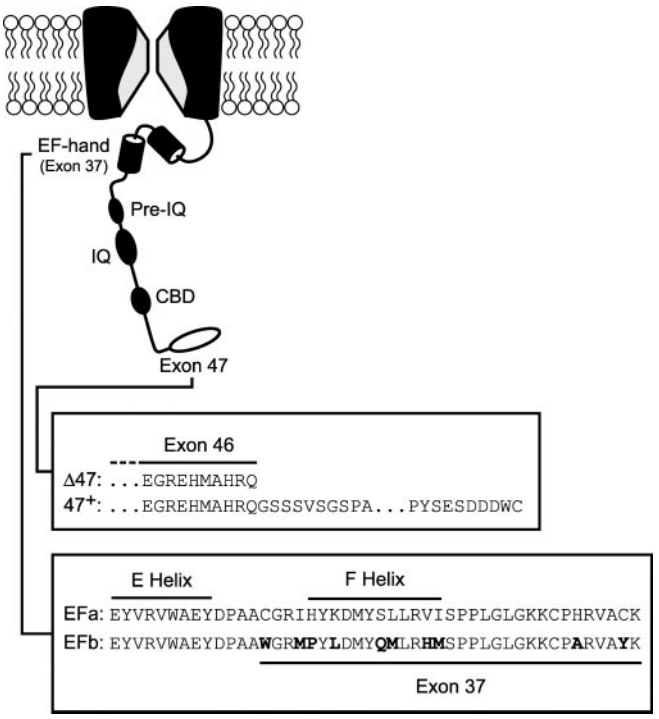

Figure 1. Structural determinants underlying CaM regulation of P/Q-type Ca^{2+} channels. The diagram depicts major elements of the P/Q-type channel carboxyl tail implicated in CaM–channel interactions underlying channel regulation. Such interactions span an IQ-like domain (IQ), a ~70 aa region upstream of the IQ (pre-IQ), and a putative CaM-binding domain (CBD) (Lee et al., 1999; DeMaria et al., 2001; Erickson et al., 2001; Lee et al., 2003). The IQ-like domain is particularly important in the CDF of channel opening. Our results here show that two additional regions, an EF-hand-like region (EF-hand) within exon 37 and the last exon (exon 47), can each modify CDF. Splice variants at these sites have been identified (Soong et al., 2002), and amino acid sequences and corresponding nomenclature for these variants are detailed in the boxes below the diagram. Differences between the EFa and EFb splice variants are in bold.

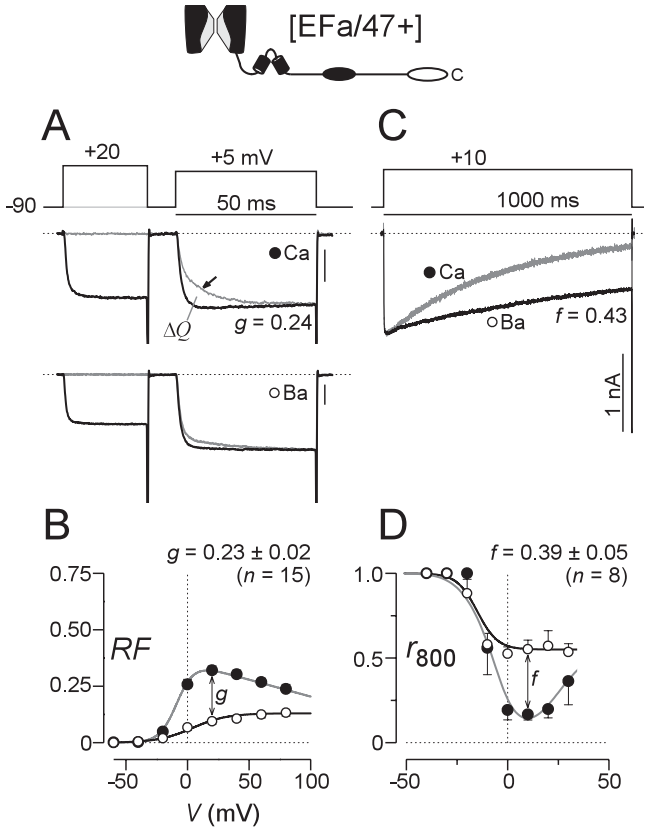

Figure 2. The [EFa/47+] splice variant shows robust CDF and CDI. *A*, Prepulse protocol characterizing CDF of [EFa/47+] channels, as expressed in HEK293 cells (top). The 50 msec test-pulse traces collected in Ca^{2+} show a slow phase of activation (arrow, middle) in the absence of a prepulse (light trace). The slow phase is abolished when the test pulse follows a prepulse (dark trace). The trace with a prepulse is scaled slightly to match the terminal phase of the test-pulse current without a prepulse. Test-pulse traces in Ba^{2+} from the same cell (bottom), showing a similar profile with (dark trace) or without (light trace) a prepulse. Format and normalization are as with Ca^{2+} traces (middle). Tail currents are clipped to frame for clarity. *B*, Fractional increase in rapidly activating test-pulse current produced by prepulse (*RF*), expressed as a function of prepulse voltage. *RF* is calculated from the area between test-pulse currents in *A*, after traces have been normalized to unity at the end of test-pulse depolarization. Symbols show averages from multiple cells, and error bars are displayed when larger than symbol size. The difference in *RF* obtained with Ba^{2+} and Ca^{2+}, as observed after a 20 mV prepulse, provides an index of pure CDF (*g*). Average *g* values ± SEM for *n* cells are shown. The *g* value for exemplar cell CDF is displayed in *A*. See supplemental information (available at www.jneurosci.org/cgi/content/full/24/28/6334/DC1) for a complete description of the analysis. *C*, CDI during a 1 sec test-pulse depolarization, seen as faster decay of Ca^{2+} versus Ba^{2+} currents. To improve visual comparison of decays, Ba^{2+} currents are scaled ~2× downward to match peak Ca^{2+} current amplitudes, here and throughout. *D*, Fraction of peak current remaining after 800 msec depolarization, r_{800}, plotted as a function of test-pulse voltage. Because CDI depends on global Ca^{2+} concentrations (Soong et al., 2002), cells with small current densities show minimal CDI. To index CDI without bias attributable to the fraction of cells with small total Ca^{2+} currents, we analyzed CDI only in cells in which Ca^{2+} current density was >40 pA/pF. Symbols are averaged from multiple cells, and error bars are displayed when larger than symbol size. To index pure CDI, we measured the difference in r_{800} obtained with Ca^{2+} and Ba^{2+} during depolarization to 10 mV (*f*). Average *f* values ± SEM for *n* cells are shown. The *f* value for exemplar cell CDI is displayed in *C*. Tail currents are clipped to frame for clarity. Calibration, 1 nA. Dotted lines show zero levels here and throughout.

ulation could be readily appreciated from a significantly greater decrease in current with Ca^{2+} rather than Ba^{2+} as the charge carrier (Fig. 2*C*). To quantify CDI, we measured the fraction of peak current remaining at 800 msec after the start of the voltage step (r_{800}). With Ca^{2+}, graphs of r_{800} plotted against the step voltage traced a classic U-shaped trajectory, characteristic of a Ca^{2+}-dependent process (Fig. 2*D*). The slower decay of Ba^{2+} currents (Fig. 2*C*) reflected a separate voltage-dependent inactivation process (Stotz and Zamponi, 2001), consistent with the monotonic decline of the Ba^{2+} r_{800} with voltage (Fig. 2*D*). To index pure CDI, then, we calculated the difference between r_{800} values for Ca^{2+} and Ba^{2+} currents evoked by 10 mV voltage steps (*f* value of ~0.39). Overall, the robust CDI and CDF of [EFa/47+] channels were very similar to those exhibited by previously characterized splice variants of P/Q-type channels (DeMaria et al., 2001; Soong et al., 2002).

In striking contrast, CDF was essentially abolished in P/Q-type channels containing α_{1A} subunits that differed only in regard to the presence of the EFb version of exon 37, [EFb/47+] (Figs. 1, 3). For this construct, Ca^{2+} currents in the absence of a prepulse lacked the slow phase of increase, showing mainly the rapidly activating component of current (Fig. 3*A*). Moreover, the test-pulse current was not significantly enhanced by a voltage prepulse, mirroring almost completely the activation pattern of Ba^{2+} currents through the same channels (data not shown). These trends were corroborated entirely by the near equivalence of averaged Ca^{2+} and Ba^{2+} *RF* relationships (*g* value of ~0.05) (Fig. 3*B*), both of which lacked the bell-shaped signature of Ca^{2+}-driven regulation. Thus, just as man-made mutations in the EF-hand region of the L-type channel could eliminate CaM-dependent regulation of that channel (Peterson et al., 2000), here a naturally occurring splice variant exerted a similar effect, acting as a molecular switch to extinguish CDF of P/Q-type channels.

Examination of CDI in these same channels [EFb/47+] pro-

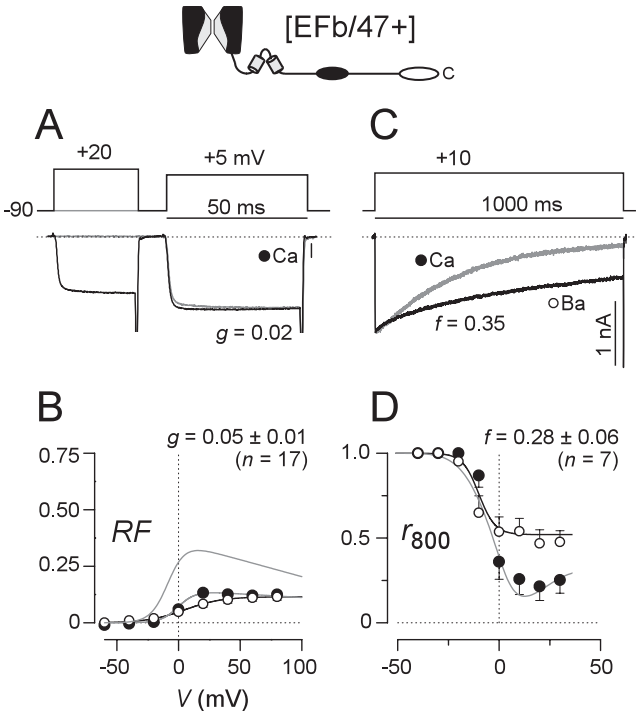

Figure 3. CDF is abolished but CDI is preserved in [EFb/47+] channels. *A–D*, Format as in Figure 2, except CDF traces for Ba^{2+} are omitted. *A*, Exemplar Ca^{2+} currents showing little or no CDF. *B*, Lack of CDF is significant compared with [EFa/47+] channels ($p < 0.01$) and confirmed by virtually identical *RF* plots for Ca^{2+} and Ba^{2+}, averaged from multiple cells. For reference, corresponding [EFa/47+] fit is reproduced as the top-most curve. *C, D*, CDI preserved at levels comparable with that in [EFa/47+] channels ($p > 0.05$).

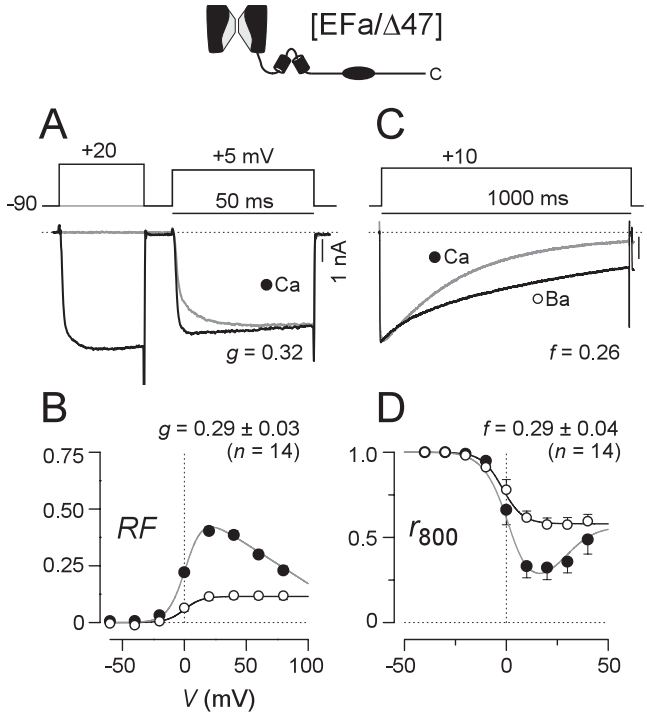

Figure 4. Robust CDF and CDI in [EFa/Δ47] channels. *A–D*, Format as in Figure 2, except CDF traces for Ba^{2+} are omitted. $p > 0.05$ compared with [EFa/47+] for CDF and CDI.

vided another valuable perspective on the functional impact of splice variation at the EF-hand locus. Despite common reliance of CDI and CDF on an IQ-like element in the α_{1A} carboxyl tail (Fig. 1) (DeMaria et al., 2001), the presence of the EFb version of exon 37 entirely spared the CDI mechanism (*f* value of ~0.28) (Fig. 3*C,D*). Hence, splice variation in the EF-hand segment of P/Q-type channels switches channel function with exquisite selectivity, dissecting apart CDI and CDF, two processes that have heretofore appeared to be closely linked (Lee et al., 1999; DeMaria et al., 2001).

Combinatorial effects of alternative splicing at exons 37 and 47

The effects of splice variation could be enriched if a specific function of a molecule were specified, not by the outcome of splicing at one locus, but collectively by the outcome at multiple loci (Mittman et al., 1999a,b). We thus considered whether the identity of the terminal stretch of the α_{1A} carboxyl tail might modulate the effects of EF-hand splicing, given that the terminus probably interacts with various adaptor proteins to organize channels in variable clusters and local environments (Maximov et al., 1999; Maximov and Bezprozvanny, 2002; Spafford et al., 2003; Weick et al., 2003). For P/Q-type channels, the terminus of the α_{1A} carboxyl tail is determined by the choice of splice acceptor site near the beginning of exon 47 (Fig. 1) (Soong et al., 2002). Splicing just before the intron 46/exon 47 border yields a transcript in which exon 47 is translated to produce a long C terminus, [47+]; splicing right at the border places an in-frame stop codon right after exon 46, yielding a shorter C terminus, [Δ47]. In the data presented thus far, EF-hand splicing was always examined in the context of the longer carboxyl tail, [47+]. Would substitution of the shorter carboxyl tail, [Δ47], affect our findings?

For P/Q-type channels composed of α_{1A} subunits with the EFa version of exon 37 and the shorter carboxyl tail [EFa/Δ47], robust CDF and CDI were clearly evident (Fig. 4) and were no different from those found in the presence of the longer carboxyl tail (Fig. 2). Moreover, the initial impression was that channels with the EFb version of exon 37 and the shorter carboxyl tail [EFb/Δ47] appeared to be unaffected by the identity of the distal C terminus (Fig. 5). On average, CDF was appreciably suppressed (*g* value of ~0.09) (Fig. 5*A,B*), and CDI was just as strong as seen with any of the other constructs (Fig. 5*C,D*).

However, on closer examination of the CDF manifest by [EFb/Δ47] channels, we uncovered a remarkable effect. For reference, consider the behavior of EFa splice variants when represented as a plot of facilitation strength (Fig. 6*A*, *g*) as a function of Ca^{2+} current density. This plot confirms robust CDF that is independent of current density, an outcome suggestive of modulation driven by local Ca^{2+} influx through individual channels rather than by global influx through many channels (Soong et al., 2002). At the other extreme, the corresponding plot for [EFb/47+] channels is consistent with complete elimination of CDF, as is evident from small *g* values across all current densities (Fig. 6*B*). With these reference behaviors in mind, we scrutinized [EFb/Δ47] channels from a similar perspective. To start, CDF of these channels, although strongly reduced compared with constructs with EFa, was undeniably present (Fig. 5*A,B*), with an average strength intermediate between the virtual elimination seen in [EFb/47+] channels and the robust baseline of [EFa] channels. Underlying this average was considerable heterogeneity in facilitation (Fig. 6*C*, middle and bottom). Certain cells showed minimal CDF, whereas others showed rather impressive CDF. Intriguingly, the heterogeneity was not random, but reflected a positive correlation between the strength of CDF (*g*) and Ca^{2+}

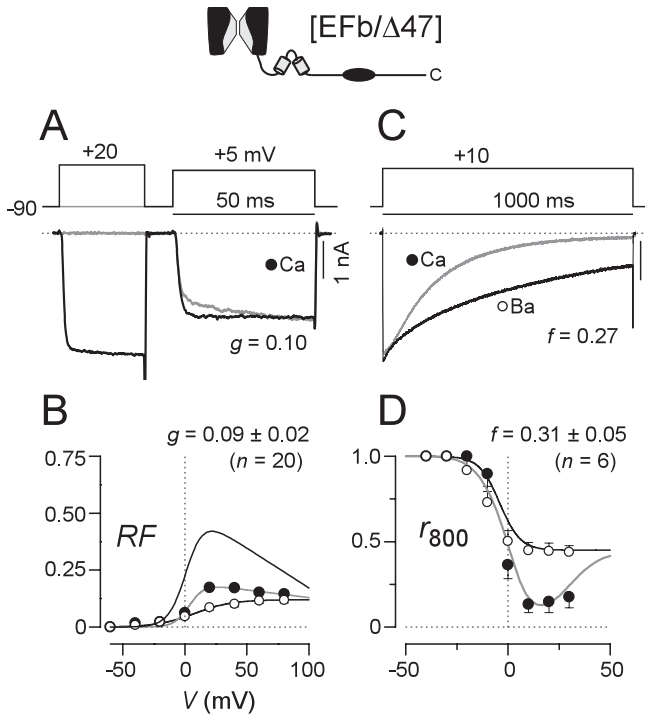

Figure 5. CDF is reduced and CDI is preserved in [EFb/Δ47] channels. *A–D*, Format as in Figure 2, except CDF traces for Ba^{2+} are omitted. *A*, Ca^{2+} currents in the absence of a prepulse (light trace) show a small facilitating component. *B*, Modest CDF is demonstrated by a diminished *RF* relationship for Ca^{2+} currents, averaged from multiple cells. For reference, the topmost curve shows the corresponding *RF* relationship for [EFa/Δ47] channels. CDF is significantly less than in [EFa/Δ47] channels ($p < 0.01$) but comparable with that in [EFb/47+] channels ($p > 0.05$). *C, D*, CDI preserved at levels comparable with that in [EFa/47+] channels ($p > 0.05$).

current density in individual cells (Fig. 6*C*). This positive correlation suggests that CDF is now driven by elevations in global Ca^{2+} influx, as represented by overall current density (Soong et al., 2002). In addition, the small *g* values at lower current densities imply that local Ca^{2+} influx through individual channels fails to induce substantial CDF in this splice variant. This profile of Ca^{2+} requirements underlying CDF is especially notable, because it suggests a novel capability of splicing: the ability to tilt the preference of a Ca^{2+} regulatory process between local and global Ca^{2+} influx. In fact, presynaptic P-type Ca^{2+} current densities can easily extend beyond 100 pA/pF (Sun and Wu, 2001), suggesting that native currents could readily induce substantial CDF driven by global Ca^{2+} activity of [EFb/Δ47] channels (Fig. 6*C*).

To substantiate further the possibility that [EFb/Δ47] channels possess CDF preferentially driven by global versus local Ca^{2+} influx, we investigated the effects of intracellular dialysis with the rapid Ca^{2+} chelator BAPTA (10 mM). This buffer should strongly suppress Ca^{2+} elevations throughout the cell interior, except within a nanodomain near the channel mouth (Naraghi and Neher, 1997; Augustine et al., 2003). Thus, CDF would persist in the presence of BAPTA only if CDF were driven preferentially by local Ca^{2+} activity; such an outcome has been observed previously for EFa splice variants (Fig. 6*D*) (Soong et al., 2002). Alternatively, if CDF is driven by global Ca^{2+} activity, little or no facilitation should be observed with BAPTA. As a check on the effectiveness of BAPTA to chelate global Ca^{2+} in the experiments here, we confirmed the complete elimination of CDI ($f = -0.02 \pm 0.02$; $n = 12$), a process previously established to require global Ca^{2+} activity (Soong et al., 2002). Under these conditions, we also observed essentially complete elimination of CDF in [EFb/Δ47] channels (*g* value of ~0.06) (Fig. 6*E*), as tested across the entire range of current densities. Overall, then, the CDF of [EFb/Δ47] channels is not switched off, but rather reprogrammed to be sensitive to global Ca^{2+} activity. In this regard, it is interesting that the CDF of presynaptic P-type currents in the calyx of Held is similarly sensitive to Ca^{2+} buffering (Borst and Sakmann, 1998; Cuttle et al., 1998), and this effect may well reflect the prevalence of [EFb/Δ47] channels at this synapse.

Prospects for EF-hand switching in native neurons

The rich functional diversity produced by alternative splicing of recombinant P/Q-type channels at exons 37 and 47 made us wonder how prevalent such splice variation might be in the nervous system. Indeed, there are indications that the rat brain shows differential expression of P/Q-type channel EF-hand variants across certain regions and developmental stages (Bourinet et al., 1999; Vigues et al., 2002). To expand this portrait of differential EF-hand expression, particularly with reference to the human context, we examined the distribution of transcripts possessing either the EFa or EFb form of exon 37 in human cDNA libraries (Fig. 7), using a PCR-based strategy. Across the entire adult brain, EFa and EFb transcripts had an almost equal distribution. This lies in stark contrast to the situation early in development, in which the brain was dominated by channels possessing the EFb variant. Additional inspection revealed that there were regional differences in the distribution of EF-hand transcripts across the adult brain. Certain areas, such as the cerebellum and hippocampus, possessed essentially equal amounts of P/Q-type channels with EFa or EFb domains. A completely new finding, unappreciated in previous screens of P/Q-type channel splice variation, concerned regions in which there was an extreme bias toward EFa or EFb. In the thalamus and substantia nigra, the EFa splice variant predominated, whereas in the amygdala, an opposite and even more extreme bias toward the EFb form was present.

In regard to alternative splicing of exon 47, our previous work with the adult human brain indicates that approximately two-thirds of α_{1A} transcripts elaborate [47+] channels, whereas the remainder of transcripts direct [Δ47] channels (Soong et al., 2002). Overall, the evidence strongly suggests that splicing of exons 37 and 47 modulates P/Q-type channel CDF across temporal and spatial dimensions in the human brain.

Discussion

Custom switching of Ca^{2+}/CaM regulation of P/Q-type channels by alternative splicing

We establish that the functional profile of a particular P/Q-type channel phenotype, Ca^{2+}-dependent facilitation, is specified by the outcome of alternative splicing at more than one locus of variation. In particular, the combinatorial effect of splicing at both exons 37 and 47 enables CDF to be modulated with exquisite selectivity among three functional settings: (1) "ON" and sensitive to local Ca^{2+} activity ([EFa/47+] or [EFa/Δ47]), (2) "partially OFF" but inducible by heightened global Ca^{2+} activity ([EFb/Δ47]), and (3) "completely OFF" ([EFb/47+]). This finding merits discussion in two regards.

First, concerning the regulatory potential of alternative splicing, functional diversity could be enriched if a particular molecular phenotype were specified by splice outcomes at more than one locus (Mittman et al., 1999a,b; Emerick et al., 2003). For example, if a single functional characteristic were specified by the outcome of splicing at a single locus, then the number of potential operational settings would be limited by the possible splice out-

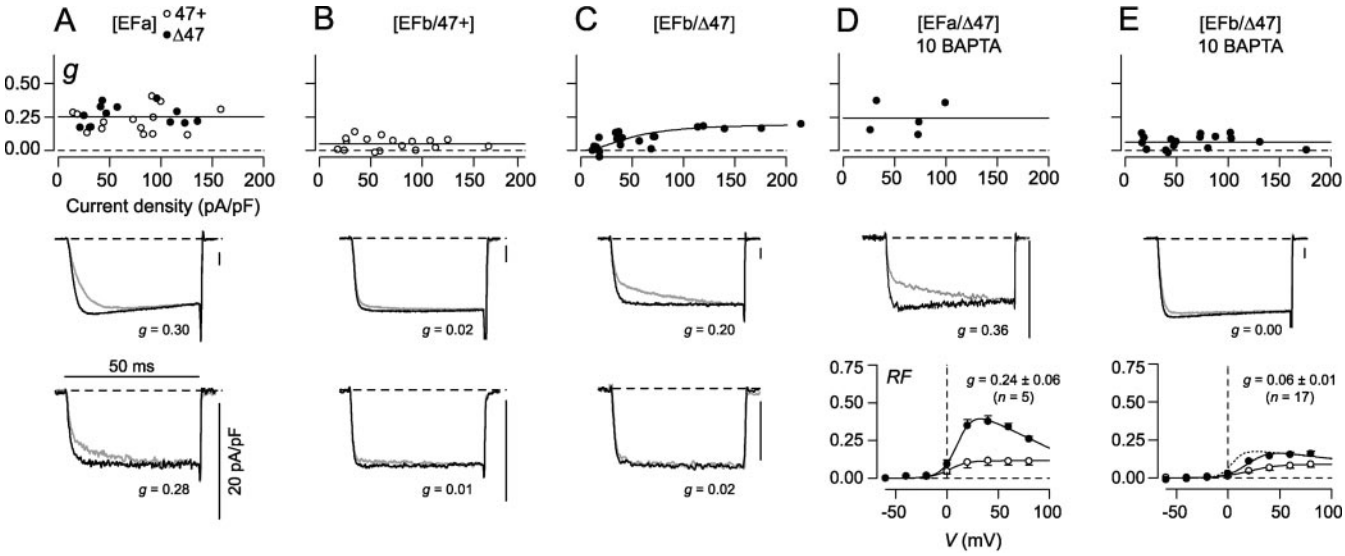

Figure 6. Current– density-dependent increase in CDF in [EFb/Δ47] channels. *A–E*, Plot of CDF strength (*g*) versus Ca^{2+} current density for the splice variant indicated at the top of each panel (top). Each symbol corresponds to an individual cell. Exemplar Ca^{2+} traces are displayed from cells with large (middle) or small (bottom) current densities, except in *D* and *E*. Shown for each splice variant are 5 mV test-pulse currents in the absence (light trace) or presence (dark trace) of a 20 mV prepulse. In *D* and *E*, a single exemplar (middle) and summary *RF* relationships (bottom) are depicted. *g* values for exemplar cells are shown with traces (middle and bottom). *A*, Although cells expressing [EFa] channels all show robust CDF, *g* does not correlate with current density, consistent with CDF driven exclusively by local Ca^{2+} entry through individual channels. *B*, [EFb/47+] channels show negligible CDF across all current densities. *C*, For cells expressing [EFb/Δ47] channels, only those with large current densities manifest appreciable CDF. Smooth curve drawn by eye. *D*, CDF is preserved in cells expressing [EFa/Δ47] channels even with increased intracellular Ca^{2+} buffering (10 mM BAPTA). Preservation of CDF is evident from the unchanged *RF* relationships for Ca^{2+} and Ba^{2+} (bottom) compared with cells recorded with minimal Ca^{2+} buffering (0.5 mM EGTA) (Fig. 4*B*). Data in *D* are reformatted from previously published data (Soong et al., 2002). *E*, Elevated intracellular Ca^{2+} buffering (10 mM BAPTA) eliminates CDF of [EFb/Δ47] channels (for current densities >45 pA/pF, $p < 0.05$ compared with [EFb/Δ47] channels recorded in 0.5 mM EGTA). Strong attenuation of CDF is confirmed by near superposition of averaged *RF* relationships for Ca^{2+} and Ba^{2+} (bottom). For reference, the top-most curve reproduces the corresponding Ca^{2+} *RF* relationship for [EFb/Δ47] channels during weak buffering of intracellular Ca^{2+} (0.5 mM EGTA, from Fig. 5*B*). Dotted lines show zero levels here and throughout.

comes at this locus (*n*). Alternatively, if molecular function were determined by splice outcomes at two loci, the number of potential functional profiles would be multiplicatively expanded to $n \times m$, where *m* is the number of variants at the second locus. Involvement of additional loci would entail additional nonlinear augmentation of the possible modes of molecular operation. The control of P/Q-type CDF by splicing at both exons 37 and 47 provides a clear-cut example of multilocus control, one with likely biological impact, as discussed later.

Second, the manner in which splice variation impacts CDF, switching its Ca^{2+} responsiveness between a preference for local versus global Ca^{2+}, represents a new dimension of modulation, as follows. It has been established recently that CaM regulation extends across virtually the entire Ca_V1–2 family of voltage-gated Ca^{2+} channels. In every case, CaM is preassociated with channels as a resident Ca^{2+} sensor (Liang et al., 2003), and each form of channel regulation is triggered preferentially by Ca^{2+} binding to one lobe of CaM but not the other. Furthermore, regardless of channel context or whether the observed Ca^{2+}-driven modulation facilitates or inactivates channel opening, a consistent pattern of CaM lobe-specific functionality has prevailed. Regulation triggered by the C-terminal lobe of CaM appears invariably insensitive to internal Ca^{2+} buffering, whereas that initiated by the N-terminal lobe is eliminated by elevated Ca^{2+} buffering with EGTA or BAPTA. From Ca^{2+} diffusion arguments (Naraghi and Neher, 1997; Song et al., 1998; DeMaria et al., 2001; Augustine et al., 2003), the implication is that the C-terminal lobe of CaM responds preferentially to the opening of its associated Ca^{2+} channel (sensitive to local Ca^{2+} influx), whereas the N-terminal lobe detects aggregate activity of more distant sources of Ca^{2+} (sensitive to global Ca^{2+} influx). For previously studied P/Q-type channels (all with EFa), this pattern has manifested as CDF driven by the C-terminal lobe of CaM and CDI induced by the N-terminal lobe of CaM (DeMaria et al., 2001). Also consistent with these findings, 10 mM BAPTA has spared P/Q-type channel CDF while eliminating CDI (Soong et al., 2002). In the present study, we encounter an initial exception to the rule, in that the CDF of [EFb/Δ47] channels (triggered by the C-terminal lobe of CaM) becomes sensitive to global Ca^{2+} influx. This may be the first example in which the preference of a resident Ca^{2+} sensor for local versus global Ca^{2+} influx has been transformed.

EF-hand domain is required for regulation by the C- but not N-terminal lobe of CaM

Regarding structure–function mechanisms underlying CaM modulation of Ca^{2+} channels, [EFb/47+] channels provide a tantalizing clue; CDF is eliminated, whereas CDI appears entirely preserved. When CDF and CDI are viewed in relation to the lobe of CaM that triggers each regulatory form, such structural selectivity hints at a general design principle for the Ca_V1–2 family. Specifically, although Ca^{2+}–CaM interactions with pre-IQ and IQ channel segments (Fig. 1) seem to be early triggers of channel regulation (Peterson et al., 2000; DeMaria et al., 2001; Liang et al., 2003), could the EF-hand domain be the general downstream transduction element for modulation by the CaM C-terminal lobe (CDF) but not the N-terminal lobe (CDI) (Fig. 8)?

Telling support comes from L-type ($Ca_V1.2$) channels, in which Ca^{2+} binding to the C-terminal lobe of CaM selectively produces CDI and man-made mutations in the EF-hand region of these channels eliminate such regulation (Peterson et al., 2000; Kim et al., 2004). No splice variation of the EF-hand region has been reported (Lipscombe and Castiglioni, 2003), because disruption of L-type channel CDI would likely have a lethal cardiac effect (Alseikhan et al., 2002). Whether the EF hand is also unim-

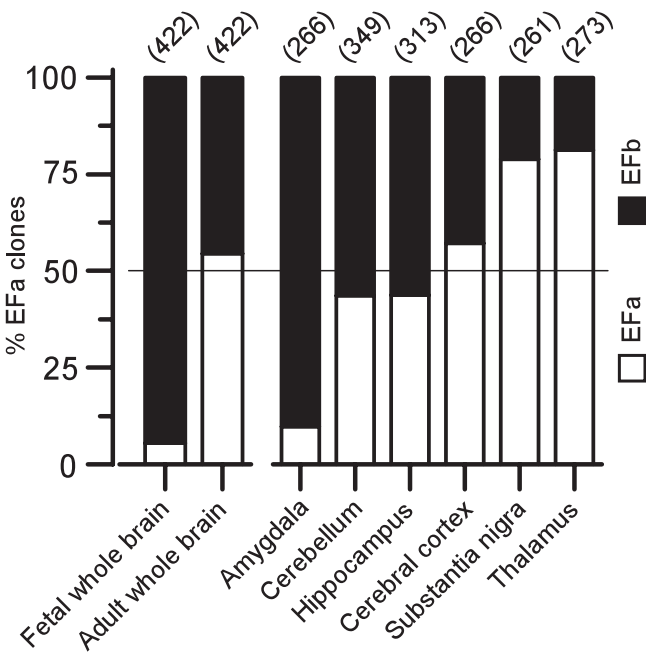

Figure 7. Prospects for neuronal control of CDF through alternative splicing. Prevalence of EF-hand splice variation in human brain, as manifest across different regions and developmental stages. The EF-hand region was amplified by PCR from the listed cDNA libraries and subcloned (see Materials and Methods); specific clones were subsequently identified as EFa or EFb. The bar graph tabulates these results, displaying the percentage of clones containing EFa versus EFb splice variants. The number of clones tallied for each library is listed in parentheses.

portant for N-terminal lobe signaling in L-type channels cannot currently be assessed, because the N-terminal lobe of CaM is not presently linked to an identifiable form of channel modulation (Peterson et al., 1999). For N- ($Ca_V2.2$) and R-type ($Ca_V2.3$) channels, however, both of which exhibit CDI triggered by the N-terminal lobe of CaM (Liang et al., 2003), the prediction is that CDI would not be affected by manipulations of their corresponding EF-hand segments. Indeed, the impact of alternative splicing of the EF-hand segment of N-type channels (Mittman and Agnew, 2000; Lipscombe et al., 2002) seems related to the overall amplitude of currents (Bell et al., 2004) rather than to a detectable change in CDI.

Beyond concerns of structure–function mechanisms, channel splice variants and mutants that selectively eliminate C- or N-terminal lobe signaling will also prove useful for neurobiological discovery. For example, to understand the biological impact of P/Q-type channel CDF, it would be advantageous to have targeted genetic means to selectively eliminate CDF without disrupting other forms of CaM regulation. Replacement of [EFa] channels by their [EFb/47+] counterparts, certainly by transgenic approaches, would serve nicely in this capacity.

Spatial and developmental control of P/Q-type channel regulation by alternative splicing

Our analysis of human mRNA transcripts (Fig. 7) suggests that both EFa and EFb versions of P/Q-type channels are likely to be prevalent and subject to considerable spatial and developmental control. We demonstrated that the distribution of splice variants encoding these channels varies systematically across different regions of the brain, as well as developmentally over time. These findings are consistent with those from rats (Bourinet et al., 1999; Vigues et al., 2002). However, our more extensive screen in humans not only amplifies these themes but also reveals some remarkable new trends. Consistent with findings in rat, human fetal whole brain shows an overwhelming presence of EFb transcripts, which transitions to an approximately equal distribution of EFa and EFb by adulthood. In adulthood, we unexpectedly discovered that certain subcortical areas (the amygdala, substantia nigra, and thalamus) manifest highly skewed distributions of EFa versus EFb transcripts (Fig. 7), suggesting that the presence of one or the other version of the EF hand is critical for proper function in these regions. Finally, although coarse developmental and regional variations in splicing are certainly observed, an even finer scale of control may be present at the level of individual neurons. For example, whereas EFa and EFb transcripts are seen in approximately equal amounts in the adult cerebellum, Purkinje cells from adult rats express predominantly EFa transcripts (Bourinet et al., 1999).

Given our functional characterization of channel splice variants, it seems likely that the purpose of variations in EFa and EFb transcripts would be to modulate channel CDF, thereby impacting neuron responsiveness to repetitive stimulation. In particular, because P/Q-type channels are enriched at presynaptic terminals (Dunlap et al., 1995) and neurotransmitter release increases with Ca^{2+} concentration by a third-to-fourth power relationship (Dodge and Rahamimoff, 1967), CDF (and preference for local or global Ca^{2+}) could significantly alter the profile of short-term synaptic plasticity. As an estimate, consider that Ca^{2+} currents through recombinant EFa channels facilitate ~20% when driven by trains of simulated action potentials (DeMaria et al., 2001), yielding a predicted enhancement of synaptic efficacy of ~200%. In contrast, the corresponding [EFb/47+] channels hardly facilitate when driven identically (data not shown), suggesting large differences in the short-term plasticity of synapses dominated by EFa versus EFb P/Q-type channels. Such increased short-term synaptic facilitation may convert synapses from detectors of changes in input firing rate ("novelty detectors") to more faithful conduits of absolute input firing rate (Tsodyks and Markram, 1997; Tsodyks et al., 1998). Enhanced short-term facilitation would also augment the efficacy of burst stimuli, a robust form of input signaling that enhances the precision of mapping location

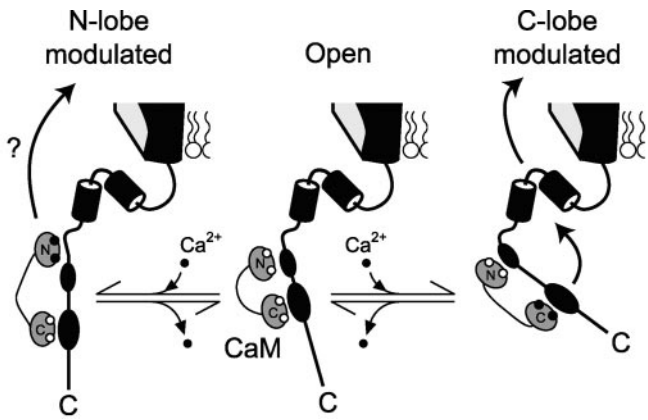

Figure 8. EF-hand domain may selectively transduce modulation by the CaM C-terminal lobe. The diagram depicts interactions proposed to underlie channel regulation by CaM. Preassociation of Ca^{2+}-free CaM with the channel IQ region is permissive for the standard open state of the channel (conducting). Ca^{2+} binding to the C-terminal lobe of CaM induces altered interaction with the IQ domain, an event that is sensed and transduced into channel modulation by the EF-hand domain (yielding CDF in P/Q-type channels and CDI in L-type channels). In contrast, Ca^{2+} binding to the N-lobe of CaM induces conformational changes that are sensed and transduced into channel modulation (CDI of N-, P/Q-, and R-type) by means that may not involve the EF-hand element.

in hippocampal place cells, and of detecting stereotyped movements in visual cortex (Lisman, 1997). Beyond information processing, P/Q-type channel activity is particularly important for the pruning of multiple climbing fibers that innervate single cerebellar Purkinje cells in neonates, which leads to the one-to-one pairing of climbing fibers and Purkinje cells in adulthood (Miyazaki et al., 2004). Because this pruning process occurs contemporaneously with the increase in EFa (Fig. 7*B*) (Vigues et al., 2002) and P/Q-type channels are unique in manifesting rapid CDF, one could hypothesize that CDF is essential for this sculpting of neuronal architecture. Testing for neurobiological consequences such as these now emerges as a critical challenge for the future.

References

Abbott LF, Varela JA, Sen K, Nelson SB (1997) Synaptic depression and cortical gain control. Science 275:220–224.

Alseikhan BA, DeMaria CD, Colecraft HM, Yue DT (2002) Engineered calmodulins reveal the unexpected eminence of Ca^{2+} channel inactivation in controlling heart excitation. Proc Natl Acad Sci USA 99:17185–17190.

Augustine GJ, Santamaria F, Tanaka K (2003) Local calcium signaling in neurons. Neuron 40:331–346.

Babitch J (1990) Channel hands. Nature 346:321–322.

Bell TJ, Thaler C, Castiglioni AJ, Helton TD, Lipscombe D (2004) Cell-specific alternative splicing increases calcium channel current density in the pain pathway. Neuron 41:127–138.

Borst JG, Sakmann B (1998) Facilitation of presynaptic calcium currents in the rat brainstem. J Physiol (Lond) 513:149–155.

Borst JG, Sakmann B (1999) Depletion of calcium in the synaptic cleft of a calyx-type synapse in the rat brainstem. J Physiol (Lond) 521:123–133.

Bourinet E, Soong TW, Sutton K, Slaymaker S, Mathews E, Monteil A, Zamponi GW, Nargeot J, Snutch TP (1999) Splicing of alpha 1A subunit gene generates phenotypic variants of P- and Q-type calcium channels. Nat Neurosci 2:407–415.

Brehm P, Eckert R (1978) Calcium entry leads to inactivation of calcium channel in *Paramecium*. Science 202:1203–1206.

Chao SH, Suzuki Y, Zysk JR, Cheung WY (1984) Activation of calmodulin by various metal cations as a function of ionic radius. Mol Pharmacol 26:75–82.

Cuttle MF, Tsujimoto T, Forsythe ID, Takahashi T (1998) Facilitation of the presynaptic calcium current at an auditory synapse in rat brainstem. J Physiol (Lond) 512:723–729.

de Leon M, Wang Y, Jones L, Perez-Reyes E, Wei X, Soong TW, Snutch TP, Yue DT (1995) Essential Ca^{2+}-binding motif for Ca^{2+}-sensitive inactivation of L-type Ca^{2+} channels. Science 270:1502–1506.

DeMaria CD, Soong TW, Alseikhan BA, Alvania RS, Yue DT (2001) Calmodulin bifurcates the local Ca^{2+} signal that modulates P/Q-type Ca^{2+} channels. Nature 411:484–489.

Dhallan RS, Yau KW, Schrader KA, Reed RR (1990) Primary structure and functional expression of a cyclic nucleotide-activated channel from olfactory neurons. Nature 347:184–187.

Dodge Jr FA, Rahamimoff R (1967) Co-operative action a calcium ions in transmitter release at the neuromuscular junction. J Physiol (Lond) 193:419–432.

Dunlap K, Luebke JI, Turner TJ (1995) Exocytotic Ca^{2+} channels in mammalian central neurons. Trends Neurosci 18:89–98.

Emerick MC, Stein R, Kunze R, Mittman S, Hanck DL, Agnew WS (2003) Recombination of subunit domains in developmentally regulated transcriptomes of CACNA1G, the human $Ca_V3.1$ calcium channel gene. Biophys J 84:329a.

Erickson MG, Alseikhan BA, Peterson BZ, Yue DT (2001) Preassociation of calmodulin with voltage-gated Ca^{2+} channels revealed by FRET in single living cells. Neuron 31:973–985.

Fletcher CF, Lutz CM, O'Sullivan TN, Shaughnessy Jr JD, Hawkes R, Frankel WN, Copeland NG, Jenkins NA (1996) Absence epilepsy in tottering mutant mice is associated with calcium channel defects. Cell 87:607–617.

Forsythe ID, Tsujimoto T, Barnes-Davies M, Cuttle MF, Takahashi T (1998) Inactivation of presynaptic calcium current contributes to synaptic depression at a fast central synapse. Neuron 20:797–807.

Glantz SA, Slinker BK (1990) Primer of applied regression and analysis of variance. New York: McGraw-Hill.

Grabowski PJ, Black DL (2001) Alternative RNA splicing in the nervous system. Prog Neurobiol 65:289–308.

Hans M, Urrutia A, Deal C, Brust PF, Stauderman K, Ellis SB, Harpold MM, Johnson EC, Williams ME (1999) Structural elements in domain IV that influence biophysical and pharmacological properties of human α_{1A}-containing high-voltage-activated calcium channels. Biophys J 76:1384–1400.

Kim J, Ghosh S, Nunziato DA, Pitt GS (2004) Identification of the components controlling inactivation of voltage-gated Ca^{2+} channels. Neuron 41:737–744.

Krovetz HS, Helton TD, Crews AL, Horne WA (2000) C-terminal alternative splicing changes the gating properties of a human spinal cord calcium channel α1A subunit. J Neurosci 20:7564–7570.

Lee A, Wong ST, Gallagher D, Li B, Storm DR, Scheuer T, Catterall WA (1999) Ca^{2+}–calmodulin binds to and modulates P/Q-type calcium channels. Nature 399:155–159.

Lee A, Scheuer T, Catterall WA (2000) Ca^{2+}–calmodulin-dependent facilitation and inactivation of P/Q-type Ca^{2+} channels. J Neurosci 20:6830–6838.

Lee A, Zhou H, Scheuer T, Catterall WA (2003) Molecular determinants of Ca^{2+}/calmodulin-dependent regulation of $Ca_v2.1$ channels. Proc Natl Acad Sci USA 100:16059–16064.

Liang H, DeMaria CD, Erickson MG, Mori MX, Alseikhan BA, Yue DT (2003) Unified mechanisms of Ca^{2+} regulation across the Ca^{2+} channel family. Neuron 39:951–960.

Ligon B, Boyd III AE, Dunlap K (1998) Class A calcium channel variants in pancreatic islets and their role in insulin secretion. J Biol Chem 273:13905–13911.

Lipscombe D, Castiglioni AJ (2003) Alternative splicing in voltage-gated calcium channels. In: Calcium channel pharmacology (McDonough SI, ed), pp 365–405. New York: Kluwer Academic/Plenum.

Lipscombe D, Pan JQ, Gray AC (2002) Functional diversity in neuronal voltage-gated calcium channels by alternative splicing of Ca(v)alpha1. Mol Neurobiol 26:21–44.

Lisman JE (1997) Bursts as a unit of neural information: making unreliable synapses reliable. Trends Neurosci 20:38–43.

Maximov A, Bezprozvanny I (2002) Synaptic targeting of N-type calcium channels in hippocampal neurons. J Neurosci 22:6939–6952.

Maximov A, Sudhof TC, Bezprozvanny I (1999) Association of neuronal calcium channels with modular adaptor proteins. J Biol Chem 274:24453–24456.

Mittman S, Agnew WS (2000) Three new alternatively spliced exons of the calcium channel alpha 1 subunit gene CACNA1B. Soc Neurosci Abstr 26:40.4.

Mittman S, Guo J, Emerick MC, Agnew WS (1999a) Structure and alternative splicing of the gene encoding alpha1I, a human brain T calcium channel alpha1 subunit. Neurosci Lett 269:121–124.

Mittman S, Guo J, Agnew WS (1999b) Structure and alternative splicing of the gene encoding alpha1G, a human brain T calcium channel alpha1 subunit. Neurosci Lett 274:143–146.

Miyazaki T, Hashimoto K, Shin HS, Kano M, Watanabe M (2004) P/Q-type Ca^{2+} channel α1A regulates synaptic competition on developing cerebellar Purkinje cells. J Neurosci 24:1734–1743.

Modrek B, Lee C (2002) A genomic view of alternative splicing. Nat Genet 30:13–19.

Mori Y, Friedrich T, Kim MS, Mikami A, Nakai J, Ruth P, Bosse E, Hofmann F, Flockerzi V, Furuichi T, Mikoshiba K, Imoto K, Tanabe T, Numa S (1991) Primary structure and functional expression from complementary DNA of a brain calcium channel. Nature 350:398–402.

Naraghi M, Neher E (1997) Linearized buffered Ca^{2+} diffusion in microdomains and its implications for calculation of $[Ca^{2+}]$ at the mouth of a calcium channel. J Neurosci 17:6961–6973.

Ophoff RA, Terwindt GM, Vergouwe MN, van Eijk R, Oefner PJ, Hoffman SM, Lamerdin JE, Mohrenweiser HW, Bulman DE, Ferrari M, Han J, Lindhout D, van Ommen GJ, Hofker MH, Ferrari MD, Frants RR (1996) Familial hemiplegic migraine and episodic ataxia type-2 are caused by mutations in the Ca^{2+} channel gene CACNL1A4. Cell 87:543–552.

Peterson BZ, DeMaria CD, Adelman JP, Yue DT (1999) Calmodulin is the Ca^{2+} sensor for Ca^{2+}-dependent inactivation of L-type calcium channels. Neuron 22:549–558.

Peterson BZ, Lee JS, Mulle JG, Wang Y, de Leon M, Yue DT (2000) Critical determinants of Ca^{2+}-dependent inactivation within an EF-hand motif of L-type Ca^{2+} channels. Biophys J 78:1906–1920.

Song LS, Sham JS, Stern MD, Lakatta EG, Cheng H (1998) Direct measurement of SR release flux by tracking "Ca^{2+} spikes" in rat cardiac myocytes. J Physiol (Lond) 512:677–691.

Soong TW, DeMaria CD, Alvania RS, Zweifel LS, Liang MC, Mittman S, Agnew WS, Yue DT (2002) Systematic identification of splice variants in human P/Q-type channel $\alpha_1$2.1 subunits: implications for current density and Ca^{2+}-dependent inactivation. J Neurosci 22:10142–10152.

Spafford JD, Munno DW, Van Nierop P, Feng ZP, Jarvis SE, Gallin WJ, Smit AB, Zamponi GW, Syed NI (2003) Calcium channel structural determinants of synaptic transmission between identified invertebrate neurons. J Biol Chem 278:4258–4267.

Starr TV, Prystay W, Snutch TP (1991) Primary structure of a calcium channel that is highly expressed in the rat cerebellum. Proc Natl Acad Sci USA 88:5621–5625.

Stotz SC, Zamponi GW (2001) Structural determinants of fast inactivation of high voltage-activated Ca^{2+} channels. Trends Neurosci 24:176–181.

Sun JY, Wu LG (2001) Fast kinetics of exocytosis revealed by simultaneous measurements of presynaptic capacitance and postsynaptic currents at a central synapse. Neuron 30:171–182.

Sutton KG, McRory JE, Guthrie H, Murphy TH, Snutch TP (1999) P/Q-type calcium channels mediate the activity-dependent feedback of syntaxin-1A. Nature 401:800–804.

Toru S, Murakoshi T, Ishikawa K, Saegusa H, Fujigasaki H, Uchihara T, Nagayama S, Osanai M, Mizusawa H, Tanabe T (2000) Spinocerebellar ataxia type 6 mutation alters P-type calcium channel function. J Biol Chem 275:10893–10898.

Tsodyks MV, Markram H (1997) The neural code between neocortical pyramidal neurons depends on neurotransmitter release probability. Proc Natl Acad Sci USA 94:719–723.

Tsodyks M, Pawelzik K, Markram H (1998) Neural networks with dynamic synapses. Neural Comput 10:821–835.

Tsunemi T, Saegusa H, Ishikawa K, Nagayama S, Murakoshi T, Mizusawa H, Tanabe T (2002) Novel Ca_v2.1 splice variants isolated from Purkinje cells do not generate P-type Ca^{2+} current. J Biol Chem 277:7214–7221.

Tufty RM, Kretsinger RH (1975) Troponin and parvalbumin calcium binding regions predicted in myosin light chain and T4 lysozyme. Science 187:167–169.

Vigues S, Gastaldi M, Massacrier A, Cau P, Valmier J (2002) The alpha(1A) subunits of rat brain calcium channels are developmentally regulated by alternative RNA splicing. Neuroscience 113:509–517.

Weick JP, Groth RD, Isaksen AL, Mermelstein PG (2003) Interactions with PDZ proteins are required for L-type calcium channels to activate cAMP response element-binding protein-dependent gene expression. J Neurosci 23:3446–3456.

Wheeler DB, Tsien RW (1999) Voltage-gated calcium channels. In: Calcium as a cellular regulator (Carafoli E, Lee C, eds), pp 171–199. New York: Oxford UP.

Wheeler DB, Randall A, Tsien RW (1994) Roles of N-type and Q-type Ca^{2+} channels in supporting hippocampal synaptic transmission. Science 264:107–111.

Zhuchenko O, Bailey J, Bonnen P, Ashizawa T, Stockton DW, Amos C, Dobyns WB, Subramony SH, Zoghbi HY, Lee CC (1997) Autosomal dominant cerebellar ataxia (SCA6) associated with small polyglutamine expansions in the alpha 1A-voltage-dependent calcium channel. Nat Genet 15:62–69.

Zuhlke RD, Reuter H (1998) Ca^{2+}-sensitive inactivation of L-type Ca^{2+} channels depends on multiple cytoplasmic amino acid sequences of the alpha1C subunit. Proc Natl Acad Sci USA 95:3287–3294.